

Valley Dependent Optoelectronics from Inversion Symmetry Breaking

Wang Yao, Di Xiao, and Qian Niu

Department of Physics, The University of Texas, Austin, TX 78712-0264

Inversion symmetry breaking allows contrasted circular dichroism in different k -space regions, which takes the extreme form of optical selection rules for interband transitions at high symmetry points. In materials where band-edges occur at noncentral valleys, this enables valley dependent interplay of electrons with light of different circular polarizations, in analogy to spin dependent optical activities in semiconductors. This discovery is in perfect harmony with the previous finding of valley contrasted Bloch band features of orbital magnetic moment and Berry curvatures from inversion symmetry breaking [Phys. Rev. Lett. **99**, 236809 (2007)]. A universal connection is revealed between the k -resolved optical oscillator strength of interband transitions, the orbital magnetic moment and the Berry curvatures, which also provides a principle for optical measurement of orbital magnetization and intrinsic anomalous Hall conductivity in ferromagnetic systems. The general physics is demonstrated in graphene where inversion symmetry breaking leads to valley contrasted optical selection rule for interband transitions. We discuss graphene based valley optoelectronics applications where light polarization information can be interconverted with electronic information.

PACS numbers: 78.67.-n, 81.05.Uw, 78.20.Ls, 85.60.-q

I. INTRODUCTION

In atoms, optical transition selection rules are determined by orbital magnetic moments of the atomic levels. Bloch bands in solids can inherit these rules from their parent atomic orbits. A well known example is the optical transition between s -like conduction and p -like valance bands in semiconductors. Strong spin-orbit coupling in the p bands mixes orbital moment with spin moment, and as a result, spin degree of freedom distinguishes two groups of electrons in their response to light with opposite circular polarizations. This forms the basis for spin optoelectronics applications in semiconductors.^{1,2,3}

In this paper, we explore an entirely different origin of selection rules and circular dichroism for optical interband transitions in solids. In addition to the intracellular current circulation of the parent atomic orbits, orbital magnetic moment of Bloch electrons has a contribution from intercellular current circulation governed by bulk symmetry properties. We show that this contribution is also tied to optical circular dichroism. When inversion symmetry is broken, contrasted circular dichroism is allowed in different regions of the Brillouin zone, which takes the extreme form of optical transition selection rules at high symmetry points.

We illustrate this general physics in graphene, the monolayer carbon honeycomb lattice recently realized in free-standing forms.^{4,5,6,7} The isolated graphene crystal-lite is a zero-gap semiconductor: the conduction and valence bands conically touch each other, forming two inequivalent valleys at the corners of the first Brillouin zone. Inversion symmetry breaking is being exploited as a powerful approach towards bandgap engineering,^{8,9,10,11,12,13} motivated by the need of semiconductor energy gap for graphene based logic devices.⁷ In graphene single layer, inversion symmetry is broken when the two sublattices become inequivalent. This effect is generally expected in epitaxially grown graphene,⁷ where

staggered sublattice potential can arise either directly from the substrate such as BN,⁸ or from a carbon buffer monolayer covalently bonded to SiC substrate.^{9,14} Recent angular resolved photo emission spectroscopy has identified mid-infrared bandgap in graphene epitaxially grown on SiC,⁹ attributed to this mechanism. In graphene bilayer, experiments and theories have revealed an energy gap continuously tunable from zero to mid-infrared by an interlayer gate bias that breaks the inversion symmetry.^{10,11,12,13} We find that at the center of the two inequivalent valleys, interband transitions couple exclusively to optical field of opposite circular polarizations.

Besides graphene, many conventional semiconductor materials have noncentral k -space valleys, e.g. Si and AlAs. Valley-based electronics applications have recently attracted great interests where this extra degree of freedom is suggested as an information carrier.^{15,16,17} In conjugation with the progressively achieved advances in piezoelectric control and magnetic control of valley degree of freedom,^{18,19,20} valley contrasted optical circular dichroism from inversion symmetry breaking creates an entirely new possibility to optically address the valley physics. This may form the basis of valley based optoelectronics applications in graphene and conventional semiconductors, in direct analogy to the well developed spin based optoelectronics.^{1,2,3}

This paper is organized as follows. In section II, a universal connection is revealed between the k -resolved optical oscillator strength of interband transitions, and the band properties of orbital magnetic moment and Berry curvatures. We show how inversion symmetry breaking allows contrasted circular dichroism for interband transitions in different regions of the Brillouin zone, which becomes a rigorous optical selection rule at high symmetry points. In section III, we demonstrate the valley contrasted optical selection rule in two qualitatively different graphene systems with broken inversion symmetry, i.e. single layer with staggered sublattice potential

and bilayer with an interlayer gate bias. In section IV, we discuss graphene based valley optoelectronics applications where light polarization information can be interconverted with electronic information. In appendix A, we give two circular dichroic sum rules for optical measurement of orbital magnetization and intrinsic anomalous Hall conductivity in ferromagnetic systems, which are direct consequence of the connection between interband optical transitions and the band topological properties discussed in section II.

II. GENERAL THEORY

We consider a non-degenerate band c for which the intracellular circulation currents from the parent atomic orbit is assumed absent.²¹ Orbital magnetic moment contributed by the intercellular current circulation can be given from the $\mathbf{k} \cdot \mathbf{p}$ analysis²²

$$\mathbf{m}(\mathbf{k}) \equiv -i \frac{e\hbar}{2m_e^2} \sum_{i \neq c} \frac{\mathcal{P}^{ci}(\mathbf{k}) \times \mathcal{P}^{ic}(\mathbf{k})}{\varepsilon_i(\mathbf{k}) - \varepsilon_c(\mathbf{k})}. \quad (1)$$

In the above, $\mathcal{P}_\alpha^{ci}(\mathbf{k}) \equiv \langle u_{c,\mathbf{k}} | \hat{p}_\alpha | u_{i,\mathbf{k}} \rangle$ is the interband matrix element of the canonical momentum operator, $\varepsilon(\mathbf{k})$ is the band dispersion, and $|u_{\mathbf{k}}\rangle$ the periodical part of the Bloch function.^{22,23} It is worth noting that this intercellular current circulation is responsible for the anomalous g -factor of electron in semiconductors: the two Bloch states with opposite spin at Γ point form a Kramer's pair with opposite \mathbf{m} which renormalize the spin Zeeman energy.²²

Now we consider the simplest situation of a two band model, where $\mathbf{m}(\mathbf{k})$ will have identical value in the upper and lower bands as evident from Eq. (1). The projection of $\mathbf{m}(\mathbf{k})$ along the light propagation direction ($\hat{\mathbf{z}}$) can be expressed as

$$-2 \frac{\mathbf{m}(\mathbf{k}) \cdot \hat{\mathbf{z}}}{\mu_B} = \frac{|\mathcal{P}_+(\mathbf{k})|^2 - |\mathcal{P}_-(\mathbf{k})|^2}{m_e (\varepsilon_c(\mathbf{k}) - \varepsilon_v(\mathbf{k}))}, \quad (2)$$

where the right hand side is the difference in k -resolved oscillator strength of $\sigma+$ and $\sigma-$ circular polarizations.²⁴ $\mathcal{P}_\pm \equiv \mathcal{P}_x^{cv} \pm i\mathcal{P}_y^{cv}$, and $\mu_B \equiv \frac{e\hbar}{2m_e}$ is the Bohr magneton of free electron. Further, with the equality for the polarization averaged oscillator strength

$$\frac{|\mathcal{P}_+(\mathbf{k})|^2 + |\mathcal{P}_-(\mathbf{k})|^2}{2m_e (\varepsilon_c(\mathbf{k}) - \varepsilon_v(\mathbf{k}))} = m_e \text{Tr} \left[\frac{1}{2} \frac{\partial^2 \varepsilon_c(\mathbf{k})}{\hbar^2 \partial k_\alpha \partial k_\beta} \right], \quad (3)$$

we find, for the interband transition at a k -space point, the degree of circular polarization is given by

$$\eta(\mathbf{k}) \equiv \frac{|\mathcal{P}_+(\mathbf{k})|^2 - |\mathcal{P}_-(\mathbf{k})|^2}{|\mathcal{P}_+(\mathbf{k})|^2 + |\mathcal{P}_-(\mathbf{k})|^2} = -\frac{\mathbf{m}(\mathbf{k}) \cdot \hat{\mathbf{z}}}{\mu_B^*(\mathbf{k})}, \quad (4)$$

where $\mu_B^*(\mathbf{k})$ is the *effective* Bohr magneton with the bare electron mass replaced by the isotropic part of the *effective mass*. Generalization of these relations to many-bands is straightforward where the contribution from

each pair of bands to the k -resolved oscillator strength and orbital magnetic moment assumes a similar relation.

Such connections open up the possibility to engineer optical circular dichroism in given bands through intercellular circulation currents determined by bulk symmetry properties. In the presence of time reversal symmetry, two Bloch states with opposite crystal momentum form a Kramer's pair with opposite orbital moment, and hence the overall circular dichroism vanishes. On the other hand, inversion symmetry dictates that a Bloch state at \mathbf{k} also has a counterpart at $-\mathbf{k}$ with identical orbital moment. Thus, inversion symmetry breaking is a necessary condition for contrasted circular dichroism in different regions of the Brillouin zone. At high symmetry points where the Bloch states are invariant under a q -fold discrete rotation about the light propagation direction: $\mathcal{R}(\frac{2\pi}{q}, \hat{\mathbf{z}}) |\psi_{c(v),\mathbf{k}}\rangle = e^{-i\frac{2\pi}{q}l_{c(v)}} |\psi_{c(v),\mathbf{k}}\rangle$, an azimuthal selection rule $l_v \pm 1 = l_c + qN$ is expected for interband transitions by light of $\sigma\pm$ circular polarization.

Berry curvature is another property that reflects handedness of Bloch electrons and it always accompanies the intercellular current circulations in the Bloch band²³

$$\mathbf{\Omega}(\mathbf{k}) \equiv i \frac{\hbar^2}{m_e^2} \sum_{i \neq c} \frac{\mathcal{P}^{ci}(\mathbf{k}) \times \mathcal{P}^{ic}(\mathbf{k})}{(\varepsilon_c(\mathbf{k}) - \varepsilon_i(\mathbf{k}))^2}. \quad (5)$$

While moving in an in-plane electric field, the carriers acquire an anomalous velocity in the transverse direction proportional to the Berry curvature, the charge and the field, giving rise to the Hall effect.^{23,25} For the two band model discussed above, we simply find

$$\eta(\mathbf{k}) = -\frac{\mathbf{m}(\mathbf{k}) \cdot \hat{\mathbf{z}}}{\mu_B^*(\mathbf{k})} = -\frac{\mathbf{\Omega}(\mathbf{k}) \cdot \hat{\mathbf{z}}}{\mu_B^*(\mathbf{k})} (\varepsilon_c(\mathbf{k}) - \varepsilon_i(\mathbf{k})) \frac{e}{2\hbar}, \quad (6)$$

where $\mathbf{m}(\mathbf{k})$ and $\mathbf{\Omega}(\mathbf{k})$ both stands for their value in the upper band (we note that $\mathbf{\Omega}(\mathbf{k})$ will have opposite value in the upper and lower bands as evident from Eq. (5)). Hence, valley contrasted optical circular dichroism is also generally accompanied by a valley contrasted contribution to the Hall conductivity. This makes possible optoelectronic schemes implementing this topological transport phenomena, as will be discussed in section IV.

In ferromagnetic systems, the universal connection between $\eta(\mathbf{k})$, $\mathbf{m}(\mathbf{k})$ and $\mathbf{\Omega}(\mathbf{k})$ directly leads to the dichroic sum rules for optical measurement of orbital magnetization and intrinsic anomalous Hall conductivity, as given in appendix A.

III. VALLEY CONTRASTED OPTICAL SELECTION RULE IN GRAPHENE

It has been shown by previous studies that a finite bandgap opens in graphene as a generic consequence of inversion symmetry breaking.^{8,9,10,11,12,13} Optical interband transitions can then be addressed in a similar way as that in conventional direct bandgap semiconductors.

The bandedges of both the conduction and valance band occur at the Dirac points which have the three-fold discrete rotational symmetry. We first demonstrate the valley contrasting selection rules in single layer graphen with staggered sublattice potential. More complex optical activities in biased graphene bilayers which enable additional optical control possibilities is presented next.

The active π bands in graphene originate from p atomic orbit with zero moment along the normal direction of the plane. The extremely weak spin-orbit coupling can be neglected.^{26,27} In the tight binding approximation graphene single layer with staggered sublattice potential can be modeled with nearest neighbor hopping energy and a site energy difference between sublattices Δ .^{8,9}

$$\hat{H}(\mathbf{k}) = \begin{bmatrix} \Delta/2 & V(\mathbf{k}) \\ V^*(\mathbf{k}) & -\Delta/2 \end{bmatrix}. \quad (7)$$

$V(\mathbf{k}) = -t(e^{i\mathbf{k}\cdot\mathbf{d}_1} + e^{i\mathbf{k}\cdot\mathbf{d}_2} + e^{i\mathbf{k}\cdot\mathbf{d}_3})$ where $\mathbf{d}_{1,2} = \frac{a}{2\sqrt{3}}\hat{x} \pm \frac{a}{2}\hat{y}$, $\mathbf{d}_3 = -\frac{a}{\sqrt{3}}\hat{x}$ with a being the lattice constant. The two component wavefunction represents the amplitude on sublattice A and B respectively. Without losing generality, we assume $\Delta > 0$, i.e. sublattice A has a larger on-site energy. Eq. (7) has the solution of a positive energy band (conduction) with dispersion $\varepsilon_c(\mathbf{k})$ and a negative energy band (valance) with dispersion $\varepsilon_v(\mathbf{k}) = -\varepsilon_c(\mathbf{k})$, separated by an energy gap of Δ . $\varepsilon_c(\mathbf{k})$ has two valleys centered at the Dirac point $\mathbf{K}_{1,2} = \mp \frac{4\pi}{3a}\hat{x}$ for which we introduce the valley index $\tau_z = \pm$. Near the Dirac points

$$|\mathcal{P}_{\pm}(\mathbf{k})|^2 = m_e^2 v_0^2 (1 \mp \tau_z \cos\theta)^2, \quad (8)$$

where $v_0 = \frac{\sqrt{3}at}{2\hbar}$ is the Fermi-Dirac velocity in graphen and $\cos\theta = \Delta/(\varepsilon_c(\mathbf{k}) - \varepsilon_v(\mathbf{k}))$. At the bottom of valley where $\varepsilon_c(\mathbf{k}) - \varepsilon_v(\mathbf{k}) \simeq \Delta$, optical transition is strongest $|\mathcal{P}|^2/m_e \sim 20$ eV, comparable to that for the transition between Γ_6 conduction and Γ_8 valance bands in GaAs. Most significantly, there is nearly perfect optical selection rule: $\sigma+$ ($\sigma-$) circularly polarized light couples only to bandedge transitions in valley K_2 (K_1) [Fig.1]. The rule is exact at the Dirac points where the conduction (valance) band state is constructed entirely from the orbits on sublattice A (B) and we have $l_c = \tau_z$ ($l_v = -\tau_z$) under the 3-fold discrete rotation (see Fig.1).²⁸ Far away from the Dirac points $\varepsilon_c(\mathbf{k}) - \varepsilon_v(\mathbf{k}) \gg \Delta$, circular dichroism disappears as in the isolated graphene sheet and we reproduce the constant high frequency optical conductivity found in Ref. 29,30.

In graphene bilayer with Bernal stacking, the A sublattice of the upper layer sits on top of the B sublattice of the lower layer. The band properties are well described by the tight-binding approximation with an intra-layer nearest neighbor hopping t , an interlayer nearest neighbor hopping t_{\perp} , and an interlayer bias Δ ,^{11,12,13}

$$H(\mathbf{k}) = \begin{bmatrix} \frac{\Delta}{2} & V(\mathbf{k}) & 0 & 0 \\ V^*(\mathbf{k}) & \frac{\Delta}{2} & t_{\perp} & 0 \\ 0 & t_{\perp} & -\frac{\Delta}{2} & V(\mathbf{k}) \\ 0 & 0 & V^*(\mathbf{k}) & -\frac{\Delta}{2} \end{bmatrix}. \quad (9)$$

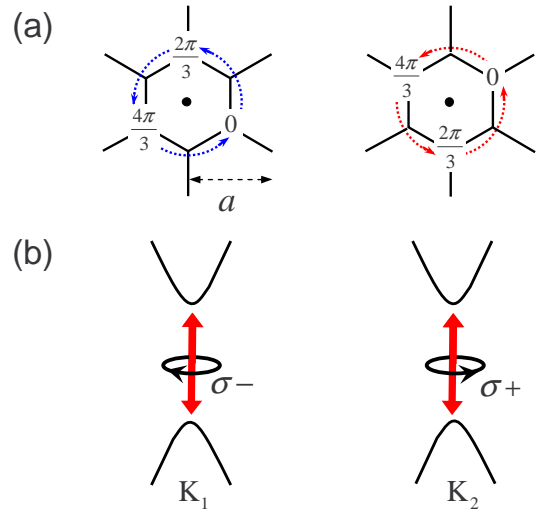


FIG. 1: (a) Left (right): phase winding of the conduction (valance) band Bloch function at $\mathbf{K}_1 = -\frac{4\pi}{3a}\hat{x}$, showing the intercellular current circulations. (b) Valley optical selection rules: $\sigma+$ ($\sigma-$) circularly polarized light couples only to band-edge transitions in valley K_2 (K_1)

The obtained band structures (see Fig. 2(a)) agree well with the measurement using angular resolved photo emission spectroscopy.¹⁰ The bilayer graphene has two positive energy bands (conduction) and two negative energy bands (valance). k -resolved oscillator strength and the degree of circular polarization are shown for interband transitions between the two conduction and the two valance bands. For the transitions between the lower conduction band and the higher valance band, a nearly perfect selection rule is obtained near the Dirac points where valley K_1 (K_2) favors $\sigma-$ ($\sigma+$) polarized light, similar to that in the graphene single layer with staggered sublattice potential. A distinct feature for this interband transition is the distribution of oscillator strength sharply concentrated at the band-edge of the Mexican hat like energy dispersion, in concert with the distribution of orbital magnetic moment and Berry curvatures found in Ref. 31. Interestingly, the transition between the two conduction bands also has a perfect selection rule but with opposite chirality in the vicinity of the Dirac points. The richer band structures and optical activities allow more optical control possibilities in bilayer graphene as discussed in section IV.

In the above, we have assumed the value of $\Delta > 0$. In the opposite case where $\Delta < 0$, the results remains the same except that the degree of the circular polarization for optical transition at each k -space point acquires a global minus sign, so that we expect the opposite transition selection rule in the two k -space valleys. Nevertheless, note that both the orbital magnetic moment and the Berry curvature acquires a global minus sign as well when Δ change sign. Thus, the optical selection rule always has the same correlation with the valley contrasted magnetic moment and the topological transport, as evi-

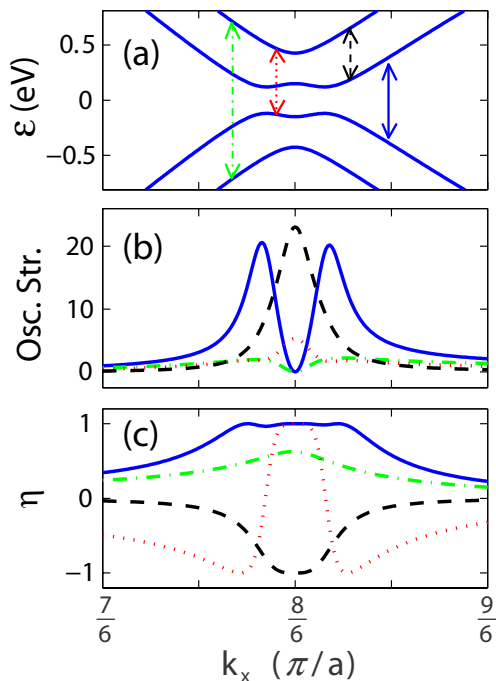


FIG. 2: (Color online) Optical properties of interband transitions in biased graphene bilayer. Energy dispersions are given in (a). k -resolved oscillator strength averaged over polarization (b), and degrees of circular polarization (c) are shown for valley K_2 . The values in valley K_1 can be obtained by noting that the oscillator strength is even while the degrees of circular polarization is odd function of \mathbf{k} . Different line style and color are used for transitions between different pairs of bands as indicated by arrowed lines in (a). The parameters used are $t = 2.82$ eV, $\Delta = 0.3$ eV, and $t_{\perp} = 0.4$ eV.

dent from Eq. (6). These physical properties in fact provide a better index for the two inequivalent valleys than the k -space positions.

IV. VALLEY OPTOELECTRONICS IN GRAPHENE

Valley optical selection rule makes possible distinct electronic response to light of different polarization, which maybe used as potential principle of light polarimetry. We give an exemplary case below exploiting the topological transport properties in graphene. Inversion symmetry breaking in graphene leads to opposite Berry curvatures distribution in the two valleys while the electrons and holes at the same k -point have the identical Berry curvatures.^{31,32} In absence of magnetic field, the net charge Hall current at equilibrium is zero as the Hall flows at the two valleys exactly cancel.^{31,33} Under the excitation by an optical field with σ^- (σ^+) polarizations, additional electrons and holes are generated in valley K_1 (K_2) and they move to opposite transverse edges of the sample if the in-plane electric field is strong enough to dissociate the electron-hole pairing (see Fig. 3(a) for an

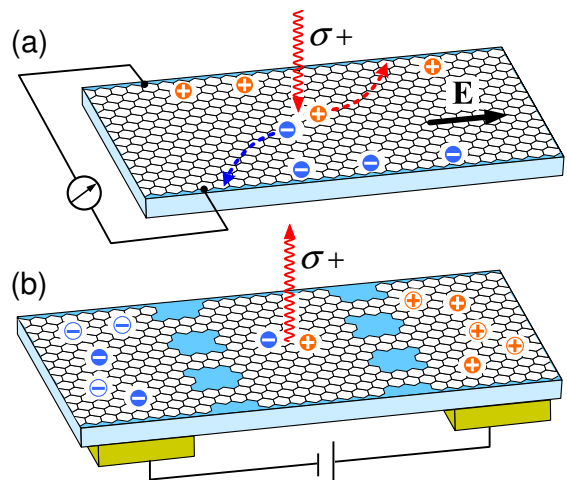


FIG. 3: (Color online) Schematic device geometry of optoelectronics based on valley contrasting optical properties of graphene. The electrons (holes) in valley K_2 are denoted by white ‘-’ (‘+’) symbol in dark circles and their counterparts in valley K_1 are denoted by inverse color. (a) Photoinduced anomalous Hall effect. (b) Valley light emitting diode. See text for the explanation of operation mechanisms.

illustration). The sign of the developed transverse voltage thus reflects the light polarization. For band-edge excitation, the photo-induced Hall conductivity in the clean limit is $\sigma_H = \pm 4\delta n \Omega_0 e^2 / h$ for σ_{\pm} polarized light, where $\Omega_0 = 2\hbar^2 v_0^2 / \Delta^2$ is the Berry curvature at the bottom of valley K_1 and δn is the density of the photo-induced valley polarized electrons/holes. In the presence of disorder, carriers may acquire an anomalous coordinate shift proportional to the Berry curvature when they scatter off an impurity potential.³⁴ This leads to a side-jump contribution to the Hall conductivity which is also independent of the scattering rate. The total Hall conductivity may have a sign change as a function of the carrier density.^{31,35} Nevertheless, even in the presence of disorders, the photo-induced Hall conductivity shall ONLY depend on the photo-induced carrier density and the magnitude of the on-site energy difference $|\Delta|$. The sign and size of the Hall voltage induced by light of certain polarization are independent of the density and details of the disorders,³⁴ and are also independent of the sign of Δ . The latter is because the relative sign between the Berry curvature and the degree of circular polarization is universal (see Eq. (6) and also the discussion in section III).

Complementarily, control of luminescence polarization by electrical means becomes possible in graphene. Mid-infrared light emitting diode (LED) with electrically controlled emission polarization can be realized in a similar fashion to the spin LED for spintronics.³ One possible configuration is shown in Fig. 3(b). The n -type and p -type regions are connected to the central intrinsic region through nano-ribbons with zigzag edges carved on the graphene sheet. These nano-ribbons act as valley filters which preferentially allow right (left) moving electrons

and left (right) moving holes in valley K_2 (K_1).¹⁶ For example, under the applied gates bias shown in Fig. 3(b), electrons tunneling leftward from the n -type region and holes tunneling rightward from the p -type region both have their majority population in the K_2 valley. In the central region, electrons and holes bound to form excitons, and radiative recombinations of these valley polarized excitons emit $\sigma+$ polarized mid-infrared photons. For SiC substrate with a dielectric constant of 10 and the resultant graphene energy gap $\Delta = 0.28$ eV,⁹ the radiative recombination time for free excitons in graphene is estimated to be $T_R \sim 10$ ps,^{36,37} much shorter than the observed intervalley scattering time $T_v \sim 100$ ps.³⁸ Reversing the gates bias leads to tunneling and recombination of electrons and holes dominantly from valley K_1 and the photon emitted from the central region will have $\sigma-$ polarization. For small carrier density, both the valley filtering effects and optical selection rules are nearly perfect. Since two intervalley scatterings are needed to bring a bright exciton from one valley to the other, we expect a polarization loss of $(T_R/T_v)^2$ by intervalley scattering.

The electrically tunable energy gap in biased graphene bilayer is a highly desirable property for optoelectronics as it enables the interplay with light of a range of frequency. At zero doping, the interband transition between the lower conduction band and upper valance band may be implemented for a valley LED with an electrically tunable emitting frequency. In metallic samples, the transition between the two conduction bands is of interest, with a peaked oscillator strength and perfect selection rules in the vicinity of the Dirac points [Fig. 2(b,c)]. The Mexican hat like dispersion in the lower conduction band further enables the frequency selectivity. Thus, photo-induced anomalous Hall effect and valley LED may also be realized in biased graphene bilayer with a large sheet density by implementing this transition between the two conduction bands.

V. CONCLUSIONS

A valley contrasting optical transition selection rule by inversion symmetry breaking is demonstrated in the exemplary system of graphene. In analogy to the spin degrees of freedom in semiconductors, the valley index in graphene distinguishes the two groups of electrons in their response to light with different circular polarizations. Hence, besides the magneto optical activities being found,^{39,40,41} graphene is of rich natural optical activities for technological interests.⁴² We show the possibility of the valley analog of spin optoelectronics in graphene. Photo-induced anomalous Hall effect^{35,43} is discussed as an example of converting light polarization information into electronic signal. Complementarily, polarization of light emission may be controlled electronically. We propose a graphene based valley LED in the mid-infrared regime, with tunability in emission frequency if realized

in biased graphene bilayer. With the usage of valley index as information carrier promised by the inefficient intervalley scattering,^{16,44,45,46} the valley selection rule can be exploited for a general class of optically controlled graphene based logic with schemes borrowed from optical control of spin information processing.^{3,47} In epitaxially grown graphene, the as-prepared samples typically have a large sheet density $n \sim 10^{12} - 10^{13}$ cm⁻².^{9,10} Adsorption of atom or molecular acceptors^{10,48} can be used in combination with gate voltage control^{4,5,6} for applications desired in the semiconducting regime.

This work is supported by the Welch Foundation, NSF under grant No. DMR-0404252/0606485, DOE under grant No. DE-FG03-02ER45958, and NSFC under grant No. 10740420252.

APPENDIX A: DICHROIC SUM RULES

Overall circular dichroism has been suggested as a probe for the orbital part of the magnetization in the literature.^{49,50,51,52} When the orbital magnetism in solids is atomic like in nature, a sum rule relates the integral of the circular dichroism to the value of the orbital magnetization in ferromagnetic systems.^{49,50} In insulators, in the presence of intercellular current circulations, it is noticed that the circular dichroism is only related to a portion of the total orbital magnetization.⁵² The universal connection between the k -resolved optical oscillator strength and the orbital magnetic moment shown in section II indicates that, in both insulators and metals, the overall interband circular dichroism shall reflect the magnetization contributed from the band orbital magnetic moment. When the contribution comes from a single band, we clearly see from Eq. (1) and (2) that

$$\frac{\mu_B}{2} (\langle f_- \rangle - \langle f_+ \rangle) = \hat{z} \cdot \int_{BZ} \frac{d\mathbf{k}}{(2\pi)^d} g(\mathbf{k}) \mathbf{m}(\mathbf{k}), \quad (\text{A1})$$

where $g(\mathbf{k})$ is the Fermi distribution function. The right hand side is simply the sum of the orbital magnetic moment of the filled states, which constitute a gauge invariant contribution to the orbital magnetization.^{53,54} $\langle f_{\pm} \rangle$ stands for the sum of the interband oscillator strength with $\sigma \pm$ polarized light respectively²⁴

$$\langle f_{\pm} \rangle \equiv \sum_i \int_{BZ} \frac{d\mathbf{k}}{(2\pi)^d} g(\mathbf{k}) \frac{|\mathcal{P}_x^{ci}(\mathbf{k}) \pm \mathcal{P}_y^{ci}(\mathbf{k})|^2}{m_e (\varepsilon_c(\mathbf{k}) - \varepsilon_i(\mathbf{k}))}. \quad (\text{A2})$$

The total orbital magnetization also includes an additional gauge invariant correction from the Berry phase effect,⁵³ which is not directly related to the circular dichroism. The sum rule revealed here clearly shows the physical significance of dividing the orbital magnetization into these two gauge invariant portions.

The sum of the Berry curvature of the filled states constitutes the intrinsic (clean limit) contribution to the anomalous Hall conductivity in ferromagnetic systems

which, in 2-dimension, is given by⁵⁵

$$\sigma_H = \frac{2e^2}{\hbar} \int_{BZ} \frac{d\mathbf{k}}{(2\pi)^2} g(\mathbf{k}) \boldsymbol{\Omega}(\mathbf{k}) \cdot \hat{z}. \quad (\text{A3})$$

The connection between the k -resolved optical oscillator strength of interband transitions and the Berry curvature makes possible optical measurement of this intrinsic con-

tribution to anomalous Hall conductivity. From Eq. (5), we find

$$\sigma_H = \frac{\epsilon_0}{\pi} \int d\omega (\epsilon_-^i(\omega) - \epsilon_+^i(\omega)), \quad (\text{A4})$$

where $\epsilon_{\pm}^i(\omega)$ is the imaginary part of the dielectric function due to interband absorptions

$$\epsilon_{\pm}^i(\omega) = \frac{\pi e^2}{\epsilon_0 m_e^2 \omega^2} \sum_i \int_{BZ} \frac{d\mathbf{k}}{(2\pi)^2} g(\mathbf{k}) |\mathcal{P}_x^{ci}(\mathbf{k}) \pm i\mathcal{P}_y^{ci}(\mathbf{k})|^2 \delta(\epsilon_c(\mathbf{k}) - \epsilon_i(\mathbf{k}) - \hbar\omega). \quad (\text{A5})$$

Eq. (A4) can be viewed as a manifestation of the Kramers-Kronig relation on the interband part of the

Hall conductivity.⁵⁵

-
- ¹ E. L. Ivchenko and G. E. Pikus, JETP Lett. **27**, 604 (1978); E. L. Ivchenko and G. E. Pikus, Sov. Phys. Semicond. **13**, 579 (1979).
- ² E. L. Ivchenko and G. E. Pikus, *Superlattices and Other Heterostructures: Symmetry and Optical Phenomena* (Springer, New York, 1997), 2nd ed.
- ³ S. A. Wolf *et al.*, Science **294**, 1488 (2001).
- ⁴ K. S. Novoselov *et al.*, Science **306**, 666 (2004).
- ⁵ K. S. Novoselov *et al.*, Nature **438**, 197 (2005).
- ⁶ Y. Zhang, Y.-W. Tan, H. L. Stormer, and P. Kim, Nature **438**, 201 (2005).
- ⁷ A. K. Geim and K. S. Novoselov, Nature Mater. **6**, 183 (2007), and references therein.
- ⁸ G. Giovannetti *et al.*, Phys. Rev. B **76**, 073103 (2007).
- ⁹ S. Y. Zhou *et al.*, Nat. Mater. **6**, 770 (2007).
- ¹⁰ T. Ohta *et al.*, Science **313**, 951 (2006).
- ¹¹ E. McCann and V. I. Fal'ko, Phys. Rev. Lett. **96**, 086805 (2006).
- ¹² E. V. Castro *et al.*, Phys. Rev. Lett. **99**, 216802 (2007).
- ¹³ H. Min, B. Sahu, S. K. Banerjee, and A. H. MacDonald, Phys. Rev. B **75**, 155115 (2007).
- ¹⁴ A. Mattausch and O. Pankratov, Phys. Rev. Lett. **99**, 076802 (2007).
- ¹⁵ O. Gunawan *et al.*, Phys. Rev. Lett. **97**, 186404 (2006).
- ¹⁶ A. Rycerz, J. Tworzydło, and C. W. J. Beenakker, Nature Phys. **3**, 172 (2007).
- ¹⁷ A. R. Akhmerov and C. W. J. Beenakker, Phys. Rev. Lett. **98**, 157003 (2007).
- ¹⁸ T. S. Lay *et al.*, Appl. Phys. Lett. **62**, 3120 (1993).
- ¹⁹ Y. P. Shkolnikov, E. P. De Poortere, E. Tutuc, and M. Shayegan, Phys. Rev. Lett. **89**, 226805 (2002).
- ²⁰ O. Gunawan *et al.*, Phys. Rev. B **74**, 155436 (2006).
- ²¹ This is the situation for the s -like conduction band in the neighborhood of the Γ point in III-V compounds, and the active π bands in graphene originated from p_z atomic orbit of carbon which has zero moment along the normal direction of the plane. Here we do not consider the degeneracy from spin, which is a dummy index in the limit of weak spin-orbit coupling. When the parent atomic orbits do contribute to the orbital magnetic moment, the Bloch bands are normally degenerate, and with large spin-orbit coupling.
- ²² Y. Yafet, in *Solid State Physics: Advances in Research and Applications* (Academic Press, 1963), vol. 14.
- ²³ M.-C. Chang and Q. Niu, Phys. Rev. B **53**, 7010 (1996).
- ²⁴ Peter. Y. Yu and Manuel Cardona *Fundamentals of Semiconductors: Physics and Materials Properties* (Springer, Berlin, 2001), 3rd ed.
- ²⁵ D. J. Thouless, M. Kohmoto, M. P. Nightingale, and M. den Nijs, Phys. Rev. Lett. **49**, 405 (1982).
- ²⁶ H. Min *et al.*, Phys. Rev. B **74**, 165310 (2006).
- ²⁷ Y. Yao *et al.*, Phys. Rev. B **75**, 041401 (2007).
- ²⁸ From Eq. (4), the selection rule at Dirac points implies that $m(\mathbf{K}_{1,2})$ is a single quantum of $\mu_B^*(\mathbf{K}_{1,2})$. In graphene single layer with a gap of 0.3 eV, the effective mass at Dirac points is $0.03m_e$ and therefore $\mu_B^* \sim 30\mu_B$.
- ²⁹ L. A. Falkovsky and A. A. Varlamov, cond-mat/0606800 (2006).
- ³⁰ V. P. Gusynin, S. G. Sharapov, and J. P. Carbotte, Phys. Rev. B **75**, 165407 (2007).
- ³¹ D. Xiao, W. Yao, and Q. Niu, Phys. Rev. Lett. **99**, 236809 (2007).
- ³² Under the particle-hole transformation, the Berry curvature changes sign. So the opposite Berry curvature for the conduction and valence electron means identical Berry curvature for conduction electron and valence hole at the same k -point.
- ³³ G. W. Semenoff, Phys. Rev. Lett. **53**, 2449 (1984).
- ³⁴ N. A. Sinitsyn *et al.*, Phys. Rev. B **72**, 045346 (2005).
- ³⁵ W. Yao, A. H. MacDonald, and Q. Niu, Phys. Rev. Lett. **99**, 047401 (2007).
- ³⁶ L. C. Andreani, Solid State Comm. **77**, 641 (1991).
- ³⁷ E. Hanamura, Phys. Rev. B **38**, 1228 (1988).
- ³⁸ R. V. Gorbachev *et al.*, Phys. Rev. Lett. **98**, 176805 (2007).
- ³⁹ D. S. L. Abergel and V. I. Fal'ko, Phys. Rev. B **75**, 155430 (2007).
- ⁴⁰ V. P. Gusynin, S. G. Sharapov, and J. P. Carbotte, Phys. Rev. Lett. **98**, 157402 (2007).

- ⁴¹ Z. Jiang *et al.*, Phys. Rev. Lett. **98**, 197403 (2007).
- ⁴² F. Wang, Y. B. Zhang, C. S. Tian, C. Girit, A. Zettl, M. Crommie, and Y. R. Shen, Science **320**, 206 (2008).
- ⁴³ X. Dai and F. C. Zhang, Phys. Rev. B **76**, 085343 (2007).
- ⁴⁴ S. V. Morozov *et al.*, Phys. Rev. Lett. **97**, 016801 (2006).
- ⁴⁵ A. F. Morpurgo and F. Guinea, Phys. Rev. Lett. **97**, 196804 (2006).
- ⁴⁶ E. McCann *et al.*, Phys. Rev. Lett. **97**, 146805 (2006).
- ⁴⁷ W. Yao, R. B. Liu, and L. J. Sham, Phys. Rev. Lett. **92**, 217402 (2004); R. B. Liu, W. Yao, and L. J. Sham, Phys. Rev. B **72**, 081306(R) (2005).
- ⁴⁸ T. O. Wehling *et al.*, cond-mat/0703390 (2007).
- ⁴⁹ B. T. Thole, P. Carra, F. Sette and G. Vanderlaan, Phys. Rev. Lett. **68**, 1943 (1992).
- ⁵⁰ M. Altarelli, Phys. Rev. B **47**, 597 (1993).
- ⁵¹ D. Y. Smith, Phys. Rev. B **13**, 157003 (1976).
- ⁵² I. Souza and D. Vanderbilt, Phys. Rev. B **77**, 054438 (2008).
- ⁵³ D. Xiao, J. Shi, and Q. Niu, Phys. Rev. Lett. **95**, 137204 (2005).
- ⁵⁴ T. Thonhauser, D. Ceresoli, D. Vanderbilt, and R. Resta, *ibid.* **95**, 137205 (2005).
- ⁵⁵ Y. Yao *et al.*, Phys. Rev. Lett. **92**, 037204 (2004).